LETTERS

Isolation of rare circulating tumour cells in cancer patients by microchip technology

Sunitha Nagrath[1]*, Lecia V. Sequist[2]*, Shyamala Maheswaran[2], Daphne W. Bell[2]†, Daniel Irimia[1], Lindsey Ulkus[2], Matthew R. Smith[2], Eunice L. Kwak[2], Subba Digumarthy[2], Alona Muzikansky[2], Paula Ryan[2], Ulysses J. Balis[1]†, Ronald G. Tompkins[1], Daniel A. Haber[2] & Mehmet Toner[1]

Viable tumour-derived epithelial cells (circulating tumour cells or CTCs) have been identified in peripheral blood from cancer patients and are probably the origin of intractable metastatic disease[1–4]. Although extremely rare, CTCs represent a potential alternative to invasive biopsies as a source of tumour tissue for the detection, characterization and monitoring of non-haematologic cancers[5–8]. The ability to identify, isolate, propagate and molecularly characterize CTC subpopulations could further the discovery of cancer stem cell biomarkers and expand the understanding of the biology of metastasis. Current strategies for isolating CTCs are limited to complex analytic approaches that generate very low yield and purity[9]. Here we describe the development of a unique microfluidic platform (the 'CTC-chip') capable of efficient and selective separation of viable CTCs from peripheral whole blood samples, mediated by the interaction of target CTCs with antibody (EpCAM)-coated microposts under precisely controlled laminar flow conditions, and without requisite pre-labelling or processing of samples. The CTC-chip successfully identified CTCs in the peripheral blood of patients with metastatic lung, prostate, pancreatic, breast and colon cancer in 115 of 116 (99%) samples, with a range of 5–1,281 CTCs per ml and approximately 50% purity. In addition, CTCs were isolated in 7/7 patients with early-stage prostate cancer. Given the high sensitivity and specificity of the CTC-chip, we tested its potential utility in monitoring response to anti-cancer therapy. In a small cohort of patients with metastatic cancer undergoing systemic treatment, temporal changes in CTC numbers correlated reasonably well with the clinical course of disease as measured by standard radiographic methods. Thus, the CTC-chip provides a new and effective tool for accurate identification and measurement of CTCs in patients with cancer. It has broad implications in advancing both cancer biology research and clinical cancer management, including the detection, diagnosis and monitoring of cancer[10].

CTCs are rare, comprising as few as one cell per 10^9 haematologic cells in the blood of patients with metastatic cancer, hence their isolation presents a tremendous technical challenge[7,9,11–13]. Microfluidic lab-on-a-chip devices provide unique opportunities for cell sorting and rare-cell detection; they have been successfully used for microfluidic flow cytometry[14], continuous size-based separation[15,16] and chromatographic separation[17]. Despite their success in manipulating microlitre amounts of simple liquids in microscale channels[14,18,19], they have thus far shown limited capability to deal with the cellular and fluid complexity of large volumes (millilitres) of whole blood samples[20–22].

Here we describe the development and application of a microfluidic device (the 'CTC-chip') that can efficiently and reproducibly isolate CTCs from the blood of patients with common epithelial tumours (Fig. 1, and Supplementary Fig. 1). The CTC-chip (Fig. 1b) consists of an array of microposts (Supplementary Fig. 1c) that are made chemically functional with anti-epithelial-cell-adhesion-molecule (EpCAM, also known as TACSTD1) antibodies. Anti-EpCAM provides the specificity for CTC capture from unfractionated blood because EpCAM is frequently overexpressed by carcinomas of lung, colorectal, breast, prostate, head and neck, and hepatic origin, and is absent from haematologic cells[23,24].

Two essential parameters that determine the efficiency of cell capture on the CTC-chip are: (1) flow velocity, because it influences the duration of cell–micropost contact; and (2) shear force, which must be sufficiently low to ensure maximum cell–micropost attachment. To optimize these parameters we employed theoretical analyses characterizing the interaction of cells with microposts distributed within

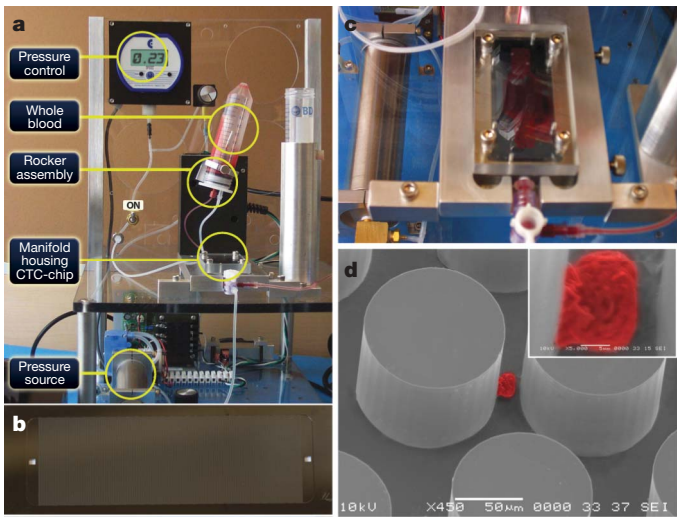

Figure 1 | Isolation of CTCs from whole blood using a microfluidic device. **a**, The workstation setup for CTC separation. The sample is continually mixed on a rocker, and pumped through the chip using a pneumatic-pressure-regulated pump. **b**, The CTC-chip with microposts etched in silicon. **c**, Whole blood flowing through the microfluidic device. **d**, Scanning electron microscope image of a captured NCI-H1650 lung cancer cell spiked into blood (pseudo coloured red). The inset shows a high magnification view of the cell.

[1]Surgical Services and BioMEMS Resource Center, Massachusetts General Hospital, Harvard Medical School, and Shriners Hospital for Children, Boston, Massachusetts 02114, USA. [2]Massachusetts General Hospital Cancer Center, Harvard Medical School, Boston, Massachusetts 02114, USA. †Present addresses: National Human Genome Research Institute/NIH Cancer Genetics Branch, Bethesda, Maryland 20892, USA (D.W.B.); Department of Pathology, University of Michigan Health System, Ann Arbor, Michigan 48109, USA (U.J.B.). *These authors contributed equally to this paper.

the flow path (Supplementary Figs 1c and 2). Briefly, the simulation indicated an equilateral triangular arrangement, with a 50 μm distance between microposts and a 50 μm shift after every 3 rows, to be the most efficient geometric arrangement. For a given volumetric flow rate of 1 ml h^{-1} through the device, the maximum shear stress experienced by a cell near the micropost surface was estimated to be 0.4 dyn cm^{-2} at $\theta = 68^{o}$ and the expected maximum velocity was 460 μm s^{-1} (Supplementary Fig. 2b–d), within the range facilitating maximum cell attachment according to linear shear stress chamber studies (Supplementary Fig. 3). On the basis of the simulation results, we fabricated a CTC-chip containing an array of 78,000 microposts within a 970 mm^2 surface.

To determine the efficiency of capture, we spiked non-small-cell lung cancer (NSCLC) cells (NCI-H1650) into phosphate buffered saline (PBS) at 100 cells ml^{-1} and captured the spiked cancer cells using the CTC-chip. NSCLC cells were visually evident about EpCAM-coated microposts, whereas no cancer cells were seen following flow through uncoated posts (Supplementary Fig. 4a–c). The calculated capture efficiency was 65% and decreased significantly at flow rates above 2.5 ml h^{-1} (Fig. 2a), presumably owing to increased shear stress, consistent with our simulation predictions. The efficiency of capture was not enhanced at flow rates less than 0.75 ml h^{-1}, leading us to select a flow rate of 1–2 ml h^{-1} for subsequent studies.

To determine the effect of cellular EpCAM expression on efficiency of CTC capture, we compared capture rates among cancer cell lines with varied EpCAM expression, including NSCLC NCI-H1650 cells and breast cancer SKBr-3 cells, with >500,000 antigens per cell; prostate cancer PC3-9 cells, with approximately 50,000 antigens per cell; and bladder cancer T-24 cells, with approximately 2,000 antigens per cell[25]. Each cell line was spiked into PBS at a concentration of 100 cells ml^{-1} and analysed, resulting in a mean capture yield of > 65% in all cases (Fig. 2b). Interestingly T-24 cells with relatively low EpCAM expression were captured as efficiently as high-level antigen-expressing cells. We believe this is due to the augmented cell–substrate interactions inherent within the CTC-chip.

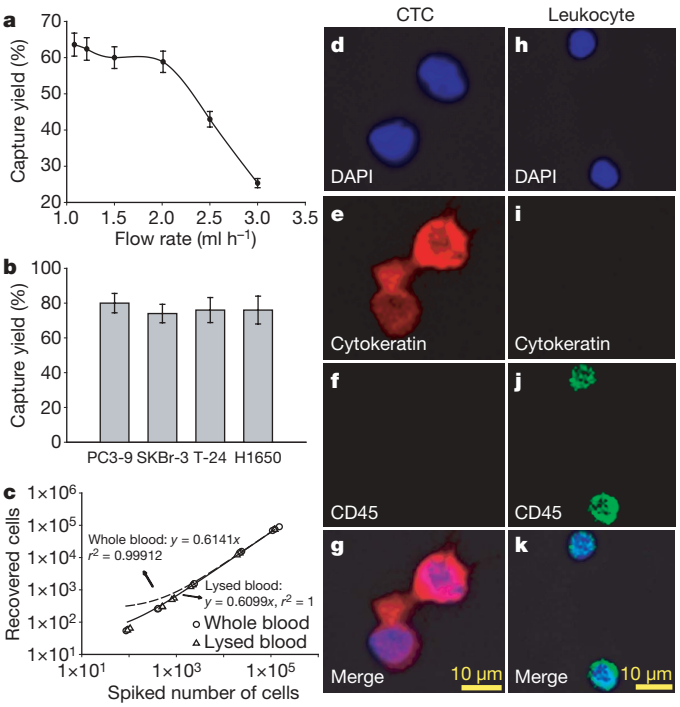

Figure 2 | CTC capture and enumeration. a, Capture yield as a function of flow rate. Data shown represent measurements averaged over three devices, and each error bar represents the standard error of the mean. **b**, Capture yields from buffer spiked with 100 cells per ml of four different cell lines: prostate (PC3-9), breast (SkBr-3), bladder (T-24), and NSCLC (NCI-H1650). Each data point was repeated in at least 3 devices. The error bars represent standard deviations of measurements within each experiment. **c**, Regression analysis of capture efficiency for various target cell concentrations, comparing whole blood to lysed blood samples. The plot represents number of cells spiked versus number of cells recovered. **d–k**, Higher magnification (20×) images of captured CTCs and haematologic cells from NSCLC patients, stained with DAPI, and for cytokeratin and CD45. Merged images identify CTCs in panels **d–g** and haematologic cells in panels **h–k**.

To evaluate cell capture under more physiological conditions, we conducted a series of experiments in which NCI-H1650 cells were spiked into whole blood from healthy donors. Suspensions at concentrations ranging from 50 to 50,000 tumour cells per ml of whole blood were analysed, yielding recovery rates of >60% in all cases (Fig. 2c). To assess the potential steric hindrance of red blood cells in the flow path, these studies were repeated using lysed blood from healthy donors. Capture rates were comparable under both conditions ($r^2 = 0.99$; Fig. 2c). Similar results were obtained using whole blood and lysed samples from NSCLC patients (Supplementary Fig. 4d, e). We thus concluded that the CTC-chip does not require blood-sample pre-processing.

Having optimized the CTC-chip with controlled quantities of cancer-derived cells, we tested its capacity to capture CTCs from whole blood samples donated by cancer patients. A total of 116 samples from 68 patients with epithelial cancers including NSCLC ($n = 55$), prostate ($n = 26$), pancreatic ($n = 15$), breast ($n = 10$) and colon ($n = 10$) were studied. The majority of patients had metastatic disease; however, 7 of 26 subjects with prostate cancer had untreated, clinically localized disease with specimens collected before prostatectomy with curative intent (Supplementary Table 2). The average volume of blood analysed was 2.7 ml per sample (range, 0.9 to 5.1 ml). We also examined samples from 20 healthy individuals (3.0 ± 0.4 ml (mean ± s.d.) of blood per subject) as controls (Supplementary Table 1).

CTCs captured from a group of patient samples were identified using a comprehensive image analysis algorithm, consisting of staining with 4,6-diamidino-2-phenylindole (DAPI) for DNA content, and using rhodamine-conjugated anti-cytokeratin (also known as KERSMCR) antibodies for epithelial cells, and fluorescein-conjugated anti-CD45 antibodies for haematologic cells (Fig. 2d–k, and Supplementary Fig. 5). Cells captured by anti-EpCAM-coated microposts and staining for cytokeratin were scored as CTCs, whereas CD45-positive cells were scored as contaminating normal haematologic cells. The morphologic characteristics exhibited by the captured CTCs were consistent with malignant cells, including large cellular size with high nuclear:cytoplasmic ratios and visible nucleoli (Fig. 2d–g). The mean viability of captured cells was 98.5 ± 2.3% (mean ± s.d.), determined by assessing cell membrane integrity in 10 high-power fields of view per CTC-chip in 4 samples obtained from lung ($n = 2$) and prostate ($n = 2$) cancer patients.

CTCs were identified in 115 of 116 (>99%) patient samples analysed, with the single negative specimen being a small volume sample (0.9 ml) from a patient with colorectal cancer. The number of CTCs isolated ranged from 5 to 1,281 per ml for NSCLC (155 ± 236 (mean ± s.d.) CTCs per ml), 16 to 292 (86 ± 78) for metastatic prostate, 25 to 174 (94 ± 63) among localized prostate cancers, 9 to 831 (196 ± 228) for pancreatic, 5 to 176 (79 ± 52) for breast, and 42 to 375 (121 ± 127) for colorectal cancers (Fig. 3a, b). The identification of CTCs in subjects with clinically localized prostate cancer at numbers approximating those in metastatic prostate cancer patients is a novel finding enabled by the high sensitivity of our technique and warrants further study. The average purity of capture, as defined by the ratio of $cytokeratin^+$ to $CD45^+$ cells, was 52% in NSCLC, 49% in metastatic prostate, 53% in localized prostate, 53% in pancreatic, 60% in breast, and 67% in colon cancers (Fig. 3c). None of the 20 healthy subjects had any identifiable CTCs (Supplementary Table 1). On the basis of these results we calculated the sensitivity (99.1%) and

specificity (100%) of the CTC-chip across all five cancers. Finally, we evaluated the reproducibility of CTC capture using split samples and showed high experimental reproducibility ($r^2 = 0.98$; Supplementary Fig. 4f).

To determine whether captured cells are suitable for subsequent molecular analyses, we tested expression of two tumour-specific markers: prostate-specific antigen (PSA; also known as KLK3) in prostate cancer and thyroid transcription factor-1 (TTF-1; also known as NKX2-1) in lung adenocarcinoma. Specific expression of these markers was evident by immunostaining (Fig. 4a, b, d, e), and confirmed by direct lysis of captured CTCs on the microchip and PCR with reverse transcription (RT–PCR) amplification of the individual transcripts (Fig. 4c, f). Considering the ~50% purity of captured viable CTCs (two orders of magnitude higher than currently available technologies)[26], the CTC-chip provides a powerful opportunity for CTC-based molecular analyses.

To demonstrate the unique clinical potential of our approach, we evaluated the ability of changes in CTC burden to predict changes in tumour volume in cancer patients undergoing anti-cancer treatments. Patients with advanced epithelial-based malignancies that were commencing a first or second line systemic treatment regimen were eligible. Blood samples were collected at baseline and during subsequent clinic visits; the exact follow-up schedule varied between patients. Computed tomograms (CT scans) were performed at baseline and at regular intervals according to standard clinical practice. For each CT scan, we calculated the sum of the unidimensional size in centimetres of all significant and measurable tumour sites, as per the RECIST standardized system[27]. All patients with baseline and at least one follow-up CTC sample and CT scan were analysed, including patients with NSCLC ($n = 3$), colorectal ($n = 2$), pancreatic ($n = 3$) and oesophageal cancer ($n = 1$) (Fig. 3d–i). The absolute number of CTCs captured did not necessarily correspond with tumour size, and may be influenced by other factors. The correlation between per cent change in CTC quantity and per cent change in tumour size, from first to last measurement, was analysed over all 9 patients and yielded a Pearson's correlation coefficient of 0.68 ($P = 0.03$). These results from a small cohort of patients show that CTC quantity correlates reasonably well with clinical response and clinical non-response to treatment (Fig. 3d–i, and Supplementary Fig. 6), indicating that monitoring treatment response using the CTC-chip may ultimately be a powerful tool enabling accurate, early decision-making. The clinical impact of such an approach could be large, and could enable a decrease in patient exposure to toxicities from ineffective therapies and guide them towards the treatments most active against their specific tumour.

Other approaches to enrich or sort CTCs from peripheral blood have been previously published, including flow cytometry[28], immunomagnetic beads[9], high-throughput optical-imaging systems[29], and fibre optic array scanning[12]. Immunomagnetic-bead purification[1,13,30] is currently the lead technology in the clinical setting, with reported success in identifying CTCs in a portion of tested patients with lung, prostate, colon, breast and pancreatic cancer[30]. However, this approach isolates small numbers of CTCs (4 ± 24 (mean $\pm$ s.d.) per ml in lung; 11 ± 118 in breast; 10 ± 33 in prostate; and 1 ± 2 in both colorectal and pancreatic cancers)[30] with very low purity (0.01–0.1%)[26], and low yield (~20–60% of patients)[30]. The

a

Cohort	Total no. of samples	Range of CTCs per mL				Samples with >5 CTC per ml (%)
		5–20	20–50	50–100	>100	
		No. of samples (%)				
Healthy subjects	20	0	0 (0)	0 (0)	0 (0)	0
Lung cancer	55	11 (20)	11 (20)	11 (20)	22 (40)	100
Prostate cancer	19	3 (16)	8 (42)	1 (5)	7 (37)	100
Localized prostate cancer	7	0 (0)	3 (43)	0 (0)	4 (57)	100
Pancreatic cancer	15	1 (7)	3 (20)	2 (13)	9 (60)	100
Breast cancer	10	2 (20)	0 (0)	4 (40)	4 (40)	100
Colon cancer	10	0 (0)	2 (20)	4 (40)	3 (30)	90

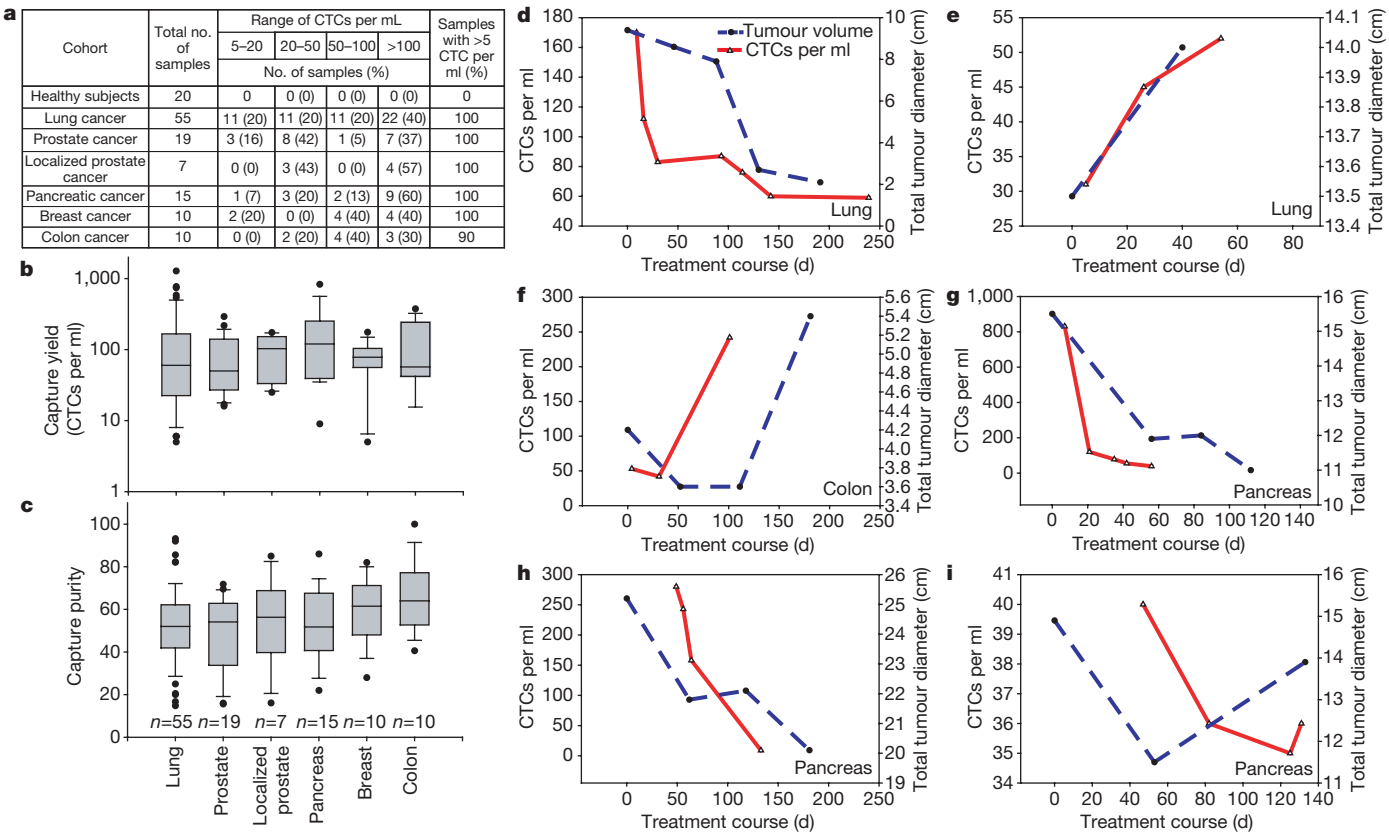

Figure 3 | Enumeration of CTCs from cancer patients. **a**, Summary of samples and CTC counts per 1 ml of blood in patients with various advanced cancers and localized prostate cancer. **b**, Frequency of CTCs per 1 ml of blood, by diagnosis. The box plot presents the median, lower and upper quartiles (25th, 75th percentiles). Data points that lie outside the 10th and 90th percentiles are shown as outliers. **c**, Purity of captured CTCs (ratio of CTCs to total nucleated cells), by diagnosis. **d–i**, Serial CTC assessment. CTC quantity (red), and tumour size (blue) measured as the unidimensional sum of all significant tumour sites on a CT scan, are well correlated over the course of anti-cancer treatment for nine patients. Six of them are shown here, for whom diagnoses and specific therapies were: NSCLC, 1st-line carboplatin, paclitaxel (**d**); NSCLC, 2nd-line pemetrexed (**e**); colorectal, 1st-line 5FU, irinotecan (**f**); pancreatic, 1st-line gemcitabine, bevacizumab (**g**); pancreatic, 1st-line gemcitabine (**h**); pancreatic, 1st-line gemcitabine, erlotinib (**i**). Baseline CT scans were before therapy initiation and CTC measurements began at or shortly after the first treatment.

level of 'biological noise' associated with the low sensitivity, selectivity, and yield of magnetic-bead-based technologies is prohibitive to their capacity to monitor response to treatment in a dynamic fashion and for early cancer detection. Hence, this method has thus far demonstrated clinical utility only as a gross prognostic tool, classifying patients into high- and low-risk categories[1]. Conversely, the high sensitivity (1 target cell in 1 billion blood cells), selectivity (>47% purity), and yield (99%) of the CTC-chip makes it ideally suited for real-time monitoring of response to cancer therapy.

In addition, the CTC-chip is unique in that it sorts rare cells directly from whole blood in a single step. From a technical perspective, this is possible because the CTC-chip is the first microfluidic device that can successfully process millilitre volumes of whole blood. This contrasts with magnetic-bead-based systems[30] that require multiple 'bulk' semi-automated preparatory steps (centrifugation, washing and incubation), resulting in loss and/or destruction of a significant proportion of the rare cells. In addition to its simplicity, the CTC-chip is readily adaptable for potential use in various clinical scenarios, including changes in throughput and in the antibody on the microposts, allowing capture of other types of rare circulating cells. The CTC-chip's one-step nature and versatility make it conducive to point-of-care use and rapid integration into clinical practice.

Finally, the CTC-chip is distinctive in that its gentle nature (maximum shear stress is 0.4 dyn cm^{-2}) allows for isolation of viable cells, whereas magnetic-bead-based approaches can only isolate fixed, non-viable cells[30]. The stationary nature of the captured cells on fixed microposts allows wash-out of non-specifically bound leukocytes, resulting in a 10^6-fold enrichment, a level of purity that is two orders of magnitude higher than existing technologies. The capacity to isolate concentrated, viable CTCs makes the CTC-chip an ideal tool for molecular access to rare CTC subpopulations such as metastatic precursor cells or cancer stem cells.

In summary, the CTC-chip captures large numbers of viable CTCs in a single step from whole blood without pre-dilution, pre-labelling, pre-fixation or any other processing steps. The techniques described here and the broader application of microfluidic rare-cell capture technology to cancer patients hold significant promise for identifying key biological determinants of blood-borne metastases, and for providing a robust platform aimed at early diagnosis and longitudinal monitoring of cancer.

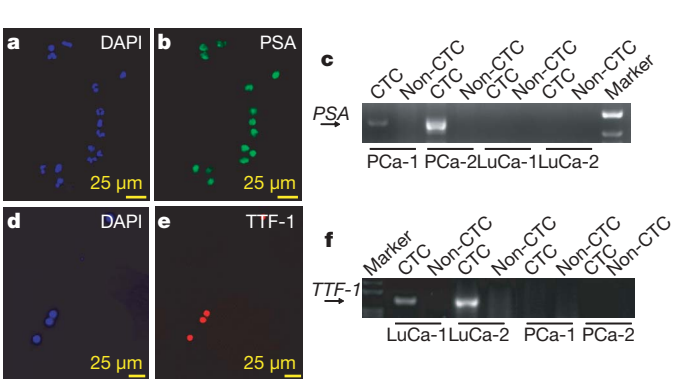

Figure 4 | Characterization of CTCs with tumour-specific molecular markers. a, **b**, CTCs from a prostate cancer patient stained positive for DAPI and PSA expression. **c**, RT–PCR amplification of *PSA* transcript is seen in two patients with prostate cancer (PCa), but not in two patients with lung cancer (LuCa), and only in blood fractions enriched for CTCs as opposed to non-enriched fractions (non-CTC). **d**, **e**, CTCs from an NSCLC patient stained for DAPI and TTF-1. **f**, RT–PCR shows expression of *TTF-1* in two patients with lung cancer (LuCa), which is absent in two patients with prostate cancer (PCa), and only when RNA was eluted from blood fractions enriched for CTCs as opposed to non-enriched fractions (non-CTC).

METHODS SUMMARY

The microfluidic system (Fig. 1a) consists of a microfluidic chip etched in silicon (Fig. 1b), a manifold to enclose the chip (Fig. 1c, and Supplementary Fig. 1b), and a pneumatic pump (Fig. 1a) to establish the flow through the capture module (Fig. 1c). The schematic of the microfluidic system is depicted in Supplementary Fig. 1b. The dimensions of the chip are 25 mm × 66 mm, with an active capture area of 19 mm × 51 mm. It contains an equilateral triangular array of microposts, 100 μm tall and 100 μm in diameter with an average 50 μm gap between microposts (Supplementary Fig. 1c). For increased hydrodynamic efficiency, the repeated patterns of equilateral triangular arrays were shifted vertically by 50 μm for every three rows throughout the chip to maximize the interactions between micropost structures and cells. This array incorporates 78,000 microposts within a surface area of 970 mm^2. Microposts were fabricated with deep reactive ion etching (DRIE) by Silex. The blood specimen collection and processing, macro-to-micro coupling, identification and enumeration of CTCs, cell viability and molecular assays are described in Methods.

Full Methods and any associated references are available in the online version of the paper at www.nature.com/nature.

Received 2 January; accepted 17 October 2007.

1. Cristofanilli, M. *et al.* Circulating tumor cells, disease progression, and survival in metastatic breast cancer. *N. Engl. J. Med.* **351,** 781–791 (2004).
2. Steeg, P. S. Tumor metastasis: mechanistic insights and clinical challenges. *Nature Med.* **12,** 895–904 (2006).
3. Gupta, G. P. & Massague, J. Cancer metastasis: building a framework. *Cell* **127,** 679–695 (2006).
4. Reya, T., Morrison, S. J., Clarke, M. F. & Weissman, I. L. Stem cells, cancer, and cancer stem cells. *Nature* **414,** 105–111 (2001).
5. Mocellin, S., Hoon, D., Ambrosi, A., Nitti, D. & Rossi, C. R. The prognostic value of circulating tumor cells in patients with melanoma: a systematic review and meta-analysis. *Clin. Cancer Res.* **12,** 4605–4613 (2006).
6. Smerage, J. B. & Hayes, D. F. The measurement and therapeutic implications of circulating tumour cells in breast cancer. *Br. J. Cancer* **94,** 8–12 (2006).
7. Rolle, A. *et al.* Increase in number of circulating disseminated epithelial cells after surgery for non-small cell lung cancer monitored by MAINTRAC(R) is a predictor for relapse: A preliminary report. *World J. Surg. Oncol.* **3,** 18 (2005).
8. Braun, S. & Marth, C. Circulating tumor cells in metastatic breast cancer—toward individualized treatment? *N. Engl. J. Med.* **351,** 824–826 (2004).
9. Zieglschmid, V., Hollmann, C. & Bocher, O. Detection of disseminated tumor cells in peripheral blood. *Crit. Rev. Clin. Lab. Sci.* **42,** 155–196 (2005).
10. Bell, D. W. & Haber, D. A. A blood-based test for epidermal growth factor receptor mutations in lung cancer. *Clin. Cancer Res.* **12,** 3875–3877 (2006).
11. Kahn, H. J. *et al.* Enumeration of circulating tumor cells in the blood of breast cancer patients after filtration enrichment: correlation with disease stage. *Breast Cancer Res. Treat.* **86,** 237–247 (2004).
12. Krivacic, R. T. *et al.* A rare-cell detector for cancer. *Proc. Natl Acad. Sci. USA* **101,** 10501–10504 (2004).
13. Racila, E. *et al.* Detection and characterization of carcinoma cells in the blood. *Proc. Natl Acad. Sci. USA* **95,** 4589–4594 (1998).
14. Fu, A. Y., Spence, C., Scherer, A., Arnold, F. H. & Quake, S. R. A microfabricated fluorescence-activated cell sorter. *Nature Biotechnol.* **17,** 1109–1111 (1999).
15. Davis, J. A. *et al.* Deterministic hydrodynamics: taking blood apart. *Proc. Natl Acad. Sci. USA* **103,** 14779–14784 (2006).
16. Huang, L. R., Cox, E. C., Austin, R. H. & Sturm, J. C. Continuous particle separation through deterministic lateral displacement. *Science* **304,** 987–990 (2004).
17. Chang, W. C., Lee, L. P. & Liepmann, D. Biomimetic technique for adhesion-based collection and separation of cells in a microfluidic channel. *Lab Chip* **5,** 64–73 (2005).
18. Whitesides, G. M. The origins and the future of microfluidics. *Nature* **442,** 368–373 (2006).
19. Hong, J. W. & Quake, S. R. Integrated nanoliter systems. *Nature Biotechnol.* **21,** 1179–1183 (2003).
20. Toner, M. & Irimia, D. Blood-on-a-chip. *Annu. Rev. Biomed. Eng.* **7,** 77–103 (2005).
21. Dittrich, P. S. & Manz, A. Lab-on-a-chip: microfluidics in drug discovery. *Nature Rev. Drug Discov.* **5,** 210–218 (2006).
22. El-Ali, J., Sorger, P. K. & Jensen, K. F. Cells on chips. *Nature* **442,** 403–411 (2006).
23. Went, P. T. *et al.* Frequent EpCam protein expression in human carcinomas. *Hum. Pathol.* **35,** 122–128 (2004).
24. Balzar, M., Winter, M. J., de Boer, C. J. & Litvinov, S. V. The biology of the 17–1A antigen (Ep-CAM). *J. Mol. Med.* **77,** 699–712 (1999).
25. Rao, C. G. *et al.* Expression of epithelial cell adhesion molecule in carcinoma cells present in blood and primary and metastatic tumors. *Int. J. Oncol.* **27,** 49–57 (2005).
26. Smirnov, D. A. *et al.* Global gene expression profiling of circulating tumor cells. *Cancer Res.* **65,** 4993–4997 (2005).
27. Therasse, P. *et al.* New guidelines to evaluate the response to treatment in solid tumors. European Organization for Research and Treatment of Cancer, National

Cancer Institute of the United States, National Cancer Institute of Canada. *J. Natl. Cancer Inst.* **92,** 205–216 (2000).
28. Terstappen, L. W. *et al.* Flow cytometry–principles and feasibility in transfusion medicine. Enumeration of epithelial derived tumor cells in peripheral blood. *Vox Sang.* **74** (suppl. 2), 269–274 (1998).
29. Kraeft, S. K. *et al.* Reliable and sensitive identification of occult tumor cells using the improved rare event imaging system. *Clin. Cancer Res.* **10,** 3020–3028 (2004).
30. Allard, W. J. *et al.* Tumor cells circulate in the peripheral blood of all major carcinomas but not in healthy subjects or patients with nonmalignant diseases. *Clin. Cancer Res.* **10,** 6897–6904 (2004).

Supplementary Information is linked to the online version of the paper at www.nature.com/nature.

Acknowledgements We thank A. Amin for technical assistance in running experiments, O. Hurtado for clean room work, S. Murthy for surface chemistry, L. Romonosky for cell counting, D. Hyde for digital pictures and D. Poulsen for illustrations. We are also grateful to R. Kapur and his team for technical assistance. The authors acknowledge funding from the National Institutes of Health (to M.T.), and the Doris Duke Distinguished Clinical Scientist Award (to D.A.H.).

Author Contributions S.N., L.V.S., R.G.T., D.A.H. and M.T. designed and conducted the study. S.M., D.W.B. and L.U. performed gene expression analyses; D.I. contributed to the microfluidic system. M.R.S., E.L.K. and P.R. acquired clinical samples. U.J.B. provided input on cytopathology; A.M. performed statistical analysis; and S.D. performed radiology measurements. S.N., L.V.S., D.W.B., S.M., D.I., D.A.H. and M.T. participated in data analysis and writing of the manuscript.

Author Information Reprints and permissions information is available at www.nature.com/reprints. The authors declare competing financial interests: details accompany the full-text HTML version of the paper at www.nature.com/nature. Correspondence and requests for materials should be addressed to M.T. (mtoner@hms.harvard.edu).

METHODS

Blood specimen collection and processing. Blood samples were drawn from patients with advanced-stage solid tumours before, during and after chemotherapy at Massachusetts General Hospital under an IRB-approved protocol. Blood specimens were also drawn from healthy donors after obtaining informed consent. All specimens were collected into vacutainer tubes containing the anticoagulant EDTA and were processed within 24 h. Between sample collection and sample processing, whole blood specimens were stored at 4 °C on a rocking platform to prevent cell settling. For experiments using lysed blood, NH_4Cl was added to whole blood in 10:1 v/v ratio and mixed for 15–20 min at room temperature. Following centrifugation at 200*g* (10 °C) for 5 min, the supernatant was removed and the pellet re-suspended in an equivalent volume of buffer and stored on a laboratory mixer at 4 °C.

Macro–micro coupling. To establish the flow through the chip, the following methods were adopted to couple the microchip with a macrofluidic pumping system. The silicon chips were purged with nitrogen and sealed with pressure-sensitive adhesive tape (3M, St Paul). The sealed microfluidic devices were then placed in a transparent 5.1 cm × 7.6 cm plastic manifold consisting of a base, top cover and a spacer (Supplementary Fig. 1b). The base has inlet and outlet ports for fluid handling. The manifold base also has six guiding metal pillars, each 1 mm in height, to hold the device in place and in alignment with the inlet and outlet ports. A metal spacer placed between the base and the top cover prevents mechanical stress on the device. The base and top cover attach by screws, providing a leak-proof assembly with minimum dead-volume. For ease of operation the port dimensions are such that standard lure fittings can be used.

A pneumatic macrofluidic drive system was specifically designed to control flow through the microfluidic CTC-chip, as shown in Fig. 1a. It uses a pneumatic pump, pressure regulators, and a digital pressure display to exquisitely control the pressure of the air used to drive blood from a sealed sample container into the CTC-chip. A rocker assembly provides sample mixing throughout the experiment. Before running samples through the chip, the device was purged with 3.0 ml of buffer. A 5 ml aliquot of blood sample was measured into a conical tube, sealed, placed on the rocker unit and connected to the capture device with low dead volume fittings (Fig. 1a). The sample was allowed to mix on the rocker for at least 5 min before running the experiment. The pneumatic pump was turned on and the pressure adjusted according to the required flow rate. After the experiment, the CTC-chip was flushed with 10.00 ml PBS at 10 ml h^{-1} to remove any non-specifically bound cells.

Identification and enumeration of CTCs by fluorescence microscopy. An Olympus SZX (Olympus America) upright reflective microscope with an automated ProScan stage (Prior Scientific) was used to image the microfluidic chip. The microchip was scanned automatically in a 1 mm × 1 mm grid format using the programmable stage and Qcapture Pro software (Media Cybernetics). Captured images (at 100× total magnification) were carefully examined and the objects that met predetermined criteria were counted. Colour, brightness and morphometric characteristics such as cell size, shape and nuclear size were considered in identifying potential CTCs and excluding cell debris and non-specific cells. Cells that stained positive for cytokeratin (cytokeratin$^+$) and met the phenotypic morphological characteristics were scored as CTCs. Cell counts were expressed as the number of cells per 1 ml of blood (CTCs per ml). Cell counts by cytokeratin$^+$ were also confirmed in a group of patients ($n = 8$) using triple stain (cytokeratin$^+$, DAPI$^+$, CD45$^-$). To evaluate inter-operator variability, the same set of scanned images from each chip ($n = 12$) was analysed by two different operators blinded to each other's results. The regression analysis of CTC counts by multiple operators demonstrated correlation coefficient (r^2) of 0.992 with a slope of 1.04, indicating that the percentage of error in counting CTCs from the images is low and that enumeration of cell counts is highly reproducible between operators.

Cell viability. Cell viability was determined with the LIVE/DEAD viability assay kit. This assay is based on intracellular esterase activity of live cells and plasma membrane integrity of dead cells. Briefly, captured CTCs were incubated at room temperature for 30 min in a solution of 2 μM calcein AM and 4 μM ethidium bromide prepared in PBS. At the end of the incubation period, the chip was washed with 1 ml of 1× PBS and visualized under the microscope.

Molecular analysis. Total RNA was isolated from cells using the Picopure RNA isolation kit according to the manufacturer's instruction and subjected to linear amplification using the TransPlex Whole Transcriptome Amplification Kit (Rubicon Genomics). The 509 base pair human PSA coding region was amplified from circulating prostate tumour cell complementary DNA using the following primer pairs (sense and antisense, 5′ to 3′): primary PCR, TTGTGGGAGGCTGGGAGTG and CCTTCTGAGGGTGAACTTGCG; secondary PCR, (GGCAGGTGCTTGTGGCCTCTCGTGG and GTCATTGGAAATAACATGGAGGTCC). The *TTF-1* transcript was amplified using the following primer pairs (sense and antisense, 5′ to 3′): primary PCR, CTGCAACGGCAACCTGGGCAACATG and CAGGTACTTCTGTTGCTTGAAGCG; secondary PCR, CAGGACACCATGAGGAACAGCGCCTC and CAGGTACTTCTGTTGCTTGAAGCG.

Modelling and theoretical device optimization. Micropost geometry and the arrangement of the micropost array were systematically explored in the process of designing the CTC-chip. Three different micropost distributions and arrangements were tested: a square array, a diagonal square array and an equilateral triangular array. The area occupied by the microposts for the square and triangular distribution is given by:

For a square array,

$$\varepsilon = \frac{\pi a^2}{l^2} \quad (1)$$

For a triangular array,

$$\varepsilon = \frac{2\pi a^2}{\sqrt{3}l^2} \quad (2)$$

Where a is the radius of the micropost and l is the centre-to-centre distance between adjacent microposts. Hence, for a given spacing between microposts, an increase in the radius of the micropost increases the micropost density, resulting in higher capture area.

The hydrodynamic efficiency for each distribution is calculated on the basis of the analytical solution derived by Drummond and Tahir[31] and is determined as the ratio of the effective capture length to the mean spacing between the microposts. The effective capture length is based on the limiting trajectory for classical interception by a cylinder calculated from the stream function. Accordingly, for an equilateral triangular distribution of microposts, the flow distribution is given by[31]:

$$U = \frac{F}{8\pi\mu}\left\{ln\left(\frac{1}{\varepsilon}\right) - 1.497504972 + 2\varepsilon - \frac{\varepsilon^2}{2} - 0.739137296\varepsilon^4 + \frac{2.534185018\varepsilon^5}{1 + 1.275793652\varepsilon}\right\} \quad (3)$$

Where U is the mean velocity between microposts, F is the force per unit length acting on the cell, μ is the fluid viscosity, and ε is as given by equation (2).

We evaluated the efficiency of cell capture using the three different micropost array distributions and found that the calculated hydrodynamic efficiency of capture as a function of the spacing between the microposts was greatest with the equilateral triangular micropost arrangement, and improved with shorter centre-to-centre spacing between the microposts (Supplementary Fig. 1a). However, excessive reduction in micropost spacing might lead to physical trapping of cells between the microposts; therefore, we selected a 50 μm distance between microposts as the calculated optimal spacing, which yields a theoretical capture efficiency of 65%. Consequently, a detailed computational analysis of the hydrodynamics (flow distribution and cell trajectories) for an equilateral triangular array distribution of microposts was performed using commercially available finite element microfluidics solver COMSOL.

To ensure the CTC-chip would be sensitive and allow for high-throughput, we employed numerical analyses using COMSOL to characterize the interaction of cells with the microposts distributed within the flow path. Two factors essential to achieve high CTC capture are: (1) optimization of flow velocity to maximize frequency of contact between cells and the chemically modified microposts, and (2) optimization of shear forces to ensure that they are lower than those favouring cell attachment to the posts. Micropost size, spacing and the distribution along the streamlines are the critical variables that determine flow velocity and shear stress. Hence, we modelled the flow properties and cell–micropost interactions for an equilateral triangular array (Supplementary Fig. 1b). We found that the triangular micropost arrangement resulted in non-linear streamlines, facilitating cell contact with micropost surfaces. For a volumetric flow rate of 1 ml h^{-1} through the device (Fig. 2a), the expected maximum velocity was 460 μm s^{-1} and occurred halfway between microposts (Supplementary Fig. 1c). We also observed that the anticipated maximum shear stress experienced by a cell near the surface of a micropost is 0.4 dyn cm^{-2} at $\theta = 68°$ (Supplementary Fig. 1d), well below the levels that are physiologically deleterious and within the range at which maximum cell attachment would be expected to occur, as determined experimentally by linear shear stress chamber studies (Supplementary Fig. 2). In summary, the analysis indicated an equilateral triangular micropost arrangement with a 50 μm distance between microposts and with a 50 μm shift after every 3 rows of microposts to be the most efficient micropost geometric arrangement and spacing. Applying a volumetric flow rate of 1 ml h^{-1} through the device yields high throughput efficient capture of cells with low non-specific binding

Making the surface functional. The CTC-chip surface was made functional with EpCAM antibodies using avidin–biotin chemistry[32]. The surface of the chip was

modified with 4% (v/v) 3-mercaptopropyl trimethoxysilane in ethanol at room temperature for 45 min, then treated with the coupling agent *N*-y-maleimidobutyryloxy succinimide ester (GMBS, 1 μM), resulting in GMBS attachment to the microposts. Next, the chip was treated with 10 μg ml^{-1} of neutravidin at room temperature for 30 min, leading to immobilization onto GMBS, and then flushed with PBS to remove excess avidin. Finally, biotinylated EpCAM antibody at a concentration of 10 μg ml^{-1} in phosphate buffered solution (PBS) with 1% (w/v) BSA and 0.09% (w/v) sodium azide was allowed to react for 15–30 min before washing with PBS. The chip was air dried and stored at ambient temperature for up to three weeks until use.

Cell-line experiments. The human non-small-cell lung cancer (NSCLC) cell line NCI-H1650 was maintained and grown to confluence in RPMI-1640 medium containing 1.5 mM L-glutamine supplemented with 10% fetal bovine serum at 37 °C in 5% CO_2, with humidity. Growth medium was aspirated and cells incubated with trypsin for 10 min. A protein buffer was added to quench protease activity. Cells were then pre-labelled with cell tracker orange using the standard protocol provided by the manufacturer. The cell titre was determined by counting with a haemocytometer. The desired concentration of cells was then prepared by serial dilution of the original cell suspension in PBS. Labelled cells were spiked into whole blood.

Fixation and staining of captured cells. Captured cells were fixed by flowing 0.9 ml of 1% PFA in PBS, through the device at 3.0 ml h^{-1} for 20 min. The chip was subsequently washed with a solution of 0.9 ml of 0.2% Triton X-100 in PBS for 10 min to induce cellular permeability and allow for intracellular staining. To identify any bound lymphocytes, 0.9 ml of anti-CD45 stock solution (50 μl of antibody stock solution in 1 ml of PBS) was passed through the chip at 3 ml h^{-1} for 30 min, followed by a PBS wash to remove excess antibody. To identify epithelial cells, 0.9 ml of anti-cytokeratin stock solution (50 μl of antibody stock solution in 1 ml of PBS) was passed through the chip at 3 ml h^{-1} for 30 min, followed by a PBS wash. Finally, to permit the identification of cellular nuclei, 0.9 ml of DAPI solution (10 μl of DAPI reagent in 1 ml of deionized water) was passed through the chip at 3 ml h^{-1}, for 15 min, followed by a PBS wash. The chip was removed from the manifold, wiped dry near the fluid ports and stored in the dark at 4 °C until imaging.

Shear stress studies using linear shear Hele-Shaw chambers. Shear stress has an important role in cell capture. An optimum shear stress should be applied such that one can capture the maximum number of cancer cells at high enough flow rates. To find the optimal flow rate, we studied the effect of shear stress on the cell capture using Hele-Shaw microfluidic chambers[32]. The geometry of these chambers (Supplementary Fig. 2d) is such that the shear stress varies linearly along the chamber length (Supplementary Fig. 2e), permitting the study of a wide range of shear stresses for a given flow rate. Cultured lung cancer cells were spiked into PBS solution, and then passed through the Hele-Shaw chambers made functional with EpCAM antibody at a constant flow rate. As the shear stress decreased along the channel, the density of the cells adhering to the micropost surface increased (Supplementary Fig. 2a–c). The effect of shear stress on cell adhesion through EpCAM antibody–antigen binding (Supplementary Fig. 2f) indicated that 8 dyn cm^{-2} was the optimum shear rate, resulting in the capture of 200 cells mm^{-2} of functionalized capture surface.

Testing CTC capture from patient blood. Before the more extensive clinical testing described in the main text, we performed initial clinical experiments using blood samples from patients with advanced NSCLC. First, we evaluated CTC capture efficiency among whole blood samples and red blood cell lysed samples in six NSCLC patients. Isolated cells are shown in Supplementary Fig. 3a. The white arrows point to CTCs and the green arrows to leukocytes. The inset at the top left of shows a high-magnification view of a cytokeratin positive (cytokeratin^{+}) CTC and the inset at the lower left presents a CD45^{+} leukocyte. The total number of cells captured for each case was analysed to calculate captured CTCs per mL of blood (Supplementary Fig. 3b). Consistent with the spiked cell experiments, we observed no significant difference in the CTC counts of cancer patients from whole blood or lysed blood, confirming that the CTC-chip can be used to isolate CTCs directly from whole blood without any need for pre-processing. The reproducibility of CTC measurements between split samples was tested with a Wilcoxon matched-pairs signed-ranks two-sided test and found to be low.

Materials. 3-Mercaptopropyl trimethoxysilane was obtained from Gelest. Ethanol (200 proof), tissue culture flasks, a haemocytometer and serological pipettes were purchased from Fisher Scientific. Fetal bovine serum (FBS) and 0.5 M ethylene diamine tetra acetic acid (EDTA) were purchased from Gibco. Dimethyl sulfoxide (DMSO), sodium azide, lyophilized bovine serum albumin (BSA) and a glovebag for handling the moisture-sensitive silane were obtained from Sigma. The coupling agent GMBS (*N*-y-maleimidobutyryloxy succinimide ester), NHS-LC-LC-biotin (succinimidyl-6¢-(biotinamido)-6-hexanamido hexanoate), and fluorescein-conjugated neutravidin were obtained from Pierce Biotechnology. Biotinylated mouse anti-human anti-EpCAM was obtained from R&D Systems. Human non-small-cell lung cancer line NCI-H1650, prostate cell line PC3-9, breast cancer cell line SKBr-3 and bladder cancer cell line T-24 were purchased from American Type Culture Collection, and RPMI-1640 growth medium was purchased from Invitrogen. Orange (5- (and 6-)-(((4-chloromethyl)-benzoyl) amino) tetramethyl-rhodamine; CMTMR) and green (5-chloromethylfluorescein diacetate; CMFDA) cell tracker dyes were obtained from Molecular Probes. Anti-cytokeratin PE (CAM 5.2, conjugated with phycoerythrin), CD45 FITC, the fluorescent nucleic acid dye nuclear dye 4′,6-diamidino-2-phenylindole (DAPI) and 10 ml vacutainer tubes were purchased from BD Biosciences.

31. Drummond, J. E. & Tahir, M. I. Laminar viscous flow through regular arrays of parallel solid cylinders. *Int. J. Multiphase Flow* **10**, 515–539 (1984).
32. Murthy, S. K., Sin, A., Tompkins, R. G. & Toner, M. Effect of flow and surface conditions on human lymphocyte isolation using microfluidic chambers. *Langmuir* **20**, 11649–11655 (2004).